Acta Pharmaceutica Sinica B 2024;14(9):3949−3963

Chinese Pharmaceutical Association
Institute of Materia Medica, Chinese Academy of Medical Sciences

Acta Pharmaceutica Sinica B

www.elsevier.com/locate/apsb
www.sciencedirect.com

ORIGINAL ARTICLE

Schisanhenol ameliorates non-alcoholic fatty liver disease *via* inhibiting miR-802 activation of AMPK-mediated modulation of hepatic lipid metabolism

Bin Li [a,†], Qi Xiao [a,†], Hongmei Zhao [b,†], Jianuo Zhang [a], Chunyan Yang [a], Yucen Zou [a], Bengang Zhang [a], Jiushi Liu [a], Haitao Sun [a,*], Haitao Liu [a,*]

[a]*State Key Laboratory of Bioactive Substance and Function of Natural Medicines, Institute of Medicinal Plant Development, Chinese Academy of Medical Sciences, Peking Union Medical College, Beijing 100193, China*
[b]*Institute of Basic Medical Sciences, Chinese Academy of Medical Sciences, Department of Pathophysiology, Peking Union Medical College, Beijing 100005, China*

Received 14 January 2024; received in revised form 25 March 2024; accepted 29 April 2024

KEY WORDS

Schisanhenol;
Non-alcoholic fatty liver disease;
Hepatic steatosis;
Lipid metabolism;
miR-802;
AMPK;
SREBP-1c;
PPARα

Abstract Non-alcoholic fatty liver disease (NAFLD), characterized by hepatic steatosis, is a common metabolic liver disease worldwide. Currently, satisfactory drugs for NAFLD treatment remain lacking. Obesity and diabetes are the leading causes of NAFLD, and compounds with anti-obesity and anti-diabetic activities are considered suitable candidates for treating NAFLD. In this study, biochemical and histological assays revealed that a natural lignan schisanhenol (SAL) effectively decreased lipid accumulation and improved hepatic steatosis in free fatty acid (FFA)-treated HepG2 cells and high-fat diet (HFD)-induced NAFLD mice. Further, molecular analyses, microRNA (miRNA)-seq, and bioinformatics analyses revealed that SAL may improve NAFLD by targeting the miR-802/adenosine monophosphate-activated protein kinase (AMPK) pathway. Liver-specific overexpression of miR-802 in NAFLD mice significantly impaired SAL-mediated liver protection and decreased the protein levels of phosphorylated (p)-AMPK and PRKAB1. Dual-luciferase assay analysis further confirmed that miR-802 inhibits hepatic AMPK expression by binding to the 3' untranslated region of mouse *Prkab1* or human *PRKAA1*.

*Corresponding authors.
E-mail addresses: htsun@implad.ac.cn (Haitao Sun), htliu@implad.ac.cn (Haitao Liu).
[†]These authors made equal contributions to this work.
Peer review under the responsibility of Chinese Pharmaceutical Association and Institute of Materia Medica, Chinese Academy of Medical Sciences.

https://doi.org/10.1016/j.apsb.2024.05.014

Additionally, genetic silencing of *PRKAA1* blocked SAL-induced AMPK pathway activation in FFA-treated HepG2 cells. The results demonstrate that SAL is an effective drug candidate for treating NAFLD through regulating miR-802/AMPK-mediated lipid metabolism.

1. Introduction

Non-alcoholic fatty liver disease (NAFLD), the most common chronic liver disease, is characterized by excessive lipid accumulation in hepatocytes[1]. NAFLD is a progressive spectrum of diseases, ranging from simple hepatic steatosis to nonalcoholic steatohepatitis, fibrosis, cirrhosis, and hepatocarcinoma[2]. Obesity and type 2 diabetes are the leading risk factors for NAFLD, and their increased prevalence has resulted in the NAFLD epidemic[3]. Currently, NAFLD affects more than 25% of the world population and is a global health concern[4]. Owing to the complex pathogenesis of NAFLD, currently satisfactory drug therapies for NAFLD remain lacking. Notably, therapeutic options are solely limited to lifestyle adjustments and indirect control drugs such as hypolipidaemic agents, insulin sensitizers, and hepatoprotectors[5]. However, prolonged adherence to these drugs is difficult for most patients and most indirect drugs are not always effective in preventing deterioration[6]. Consequently, developing new therapeutic drugs for NAFLD is urgently needed.

Although NAFLD pathogenesis remains unclear, lipid metabolism disorders are commonly involved initially and critically in its progression[7]. Increased *de novo* synthesis of fatty acids, the influx of lipids from adipose tissues, and reduced lipid decomposition can promote excessive lipid deposition in hepatocytes, resulting in hepatosteatosis[8]. Therefore, reversing hepatic lipid metabolism disorders may be an effective strategy for improving NALFD[9]. Adenosine monophosphate-activated protein kinase (AMPK), an important metabolic regulator, regulates glycolipid metabolism in hepatocytes[10]. Notably, hepatic AMPK, a factor that mainly contributes to excessive lipid deposition in the NAFLD, is attenuated in high-fat diet (HFD)-fed mice[11]. AMPK activation prevents hepatic steatosis by inhibiting fatty acid synthesis and enhancing fatty acid oxidation[8]. Furthermore, the loss of AMPK exacerbates the pathological features of NAFLD in liver-specific AMPK knockout mice[12]. Therefore, AMPK plays a key role in reducing lipid deposition and ameliorating hepatic steatosis.

Aberrantly expressed microRNAs (miRNAs) are associated with impaired AMPK function in NAFLD[13]. miRNAs are small noncoding RNAs that regulate post-transcriptional gene expression by promoting messenger RNA cleavage or inhibiting protein translation[14]. The microRNA expression profiles of patients with NAFLD and healthy individuals differ significantly, and aberrant microRNA expression critically contributes to NAFLD development and progression[14–16]. Further, clinical studies have suggested that certain miRNAs could be used as biomarkers for NAFLD diagnosis, prognosis, and treatment[17,18]. Notably, dysregulated miRNAs inhibit AMPK expression and activity in the liver, promoting NAFLD[13]. For instance, hepatic miR-33, miR-34a, miR-1224-5p, and miR-291b-3p are upregulated in NAFLD, resulting in deranged hepatic lipid metabolism and hepatic steatosis by repressing AMPK activity[13,19–21]. Conversely, inhibiting their overexpression improves AMPK activity, resulting in reduced lipid accumulation in the liver[13]. Therefore, the miRNA/AMPK axis may represent a potential therapeutic target for NAFLD treatment.

Natural products are important sources of new drugs, and compounds with anti-obesity and anti-diabetic effects may have therapeutic potential for NAFLD[3]. Schisanhenol (SAL), a biphenylcyclooctene-type lignan, is a main active ingredient of the Schisandraceous family and exhibits hepatoprotective, anti-obesity, anti-diabetic, neuroprotective, and anti-oxidant activities[22–25]. SAL exhibits a good protective effect against CCl_4-induced liver injury *in vitro* and ameliorates liver fibrosis by inhibiting hepatic stellate cell activation[26,27]. In addition, SAL analogues, such as deoxyschizandrin, schizandrin B, and gomisin J, exhibit good anti-NAFLD effects, and its analogue, gomisin M_1, exerts hepatoprotective effects in hepatocellular carcinoma by modulating miR-21[28–32]. However, whether and how SAL ameliorates NAFLD remains unknown. The present study demonstrated that SAL administration effectively improved lipid accumulation and hepatic steatosis by activating the AMPK pathway in free fatty acid (FFA)-treated HepG2 cells and HFD-fed mice. Mechanistically, SAL downregulates hepatic miR-802 expression, which directly targets mouse *Prkab1* or human *PRKAA1*, resulting in AMPK pathway activation and subsequent attenuation of hepatic lipogenesis. To our knowledge, SAL may be a novel therapeutic candidate for NAFLD.

2. Materials and methods

2.1. Chemicals and reagents

SAL (≥98% purity) was isolated from *Schisandra chinensis* fruit by our group (Supporting Information Figs. S1 and S2)[22]. Pioglitazone hydrochloride (PGZ) tablets were provided by Jiangsu Deyuan Pharmaceutical Co., Ltd. (Jiangsu, China). Alanine aminotransferase (ALT, #100020000) and aspartate aminotransferase (AST, #100020010) assay kits were purchased from Biosino Biotechnology and Science Inc. (Beijing, China). The kits used to detect triglycerides (TG, #BC0625), total cholesterol (TC, #BC1985), low-density lipoprotein cholesterol (LDL-C, #BC5335), and high-density lipoprotein cholesterol (HDL-C, #BC5325), and for Oil red O staining (#G1263) were provided by Beijing Solarbio Science Technology Co., Ltd. (Beijing, China). Dulbecco's modified Eagle's medium (#C11995500BT) and fetal bovine serum (FBS, #10099141) were purchased from Gibco (Carlsbad, CA, USA). The Cell Counting Kit-8 (CCK-8, #C0037) was purchased from Beyotime Biotechnology (Shanghai, China). The Bicinchoninic Acid (BCA) Protein Assay Kit (#23227) was obtained from Thermo Fisher Scientific (Waltham, MA, USA).

The antibody specific for phospho-AMP-activated protein kinase alpha (p-AMPK^{Thr172}) was obtained from Cell Signaling Technology (Danvers, MA, USA). Antibodies specific for AMP-activated alpha 1 (PRKAA1, #10929-2-AP), PRKAA2 (#18167-1-AP), sterol regulatory element binding protein-1c (SREBP-1c, #14088-1-AP), acetyl-CoA carboxylase (ACC, #21923-1-AP), p-ACC (#29119-1-AP), and glyceraldehyde-3-phosphate dehydrogenase (GAPDH, #10494-1-AP) were purchased from Proteintech Biotechnology (Wuhan, China). AMP-activated beta 1 (PRKAB1, #ab32112) and peroxisome proliferator-activated receptor α (PPARα, #ab227074) were obtained from Abcam (Cambridge, UK). Adeno-associated virus 8 overexpressing miR-802-5p (AAV8-pre-miR-802-5p, represented as miR-802), AAV8 overexpressing miR-802 control (AAV8-GFP), AAV8 encoding miR-802-RNA interference (AAV8-anti-miR-802), and AAV8 encoding miR-802-RNA interference control (AAV8-ctrl) were synthesized by GeneChem (Shanghai, China). miR-802 and NC inhibitors were purchased from General Biosystems (Anhui, China).

2.2. Animals

Male C57BL/6J mice (18−22 g) were obtained from Beijing Vital River Laboratory Animal Technology Co., Ltd. (Beijing, China), and housed under controlled temperature (22 ± 2 °C) and humidity (60 ± 5%) with a 12-h light/dark cycle. Food and water were freely available to all animals. Animal care and experimental protocols were conducted in compliance with the principles of the Institutional Animal Care and Use Committee at the Chinese Academy of Medical Sciences and Peking Union Medical College (Beijing, China) in accordance with the Guide for the Care and Use of Laboratory Animals (National Institutes of Health).

2.3. Establishment and treatment of the NAFLD mouse model

The NAFLD mouse model was established after 1 week of acclimatization using a HFD (10% lard, 1% cholesterol, 10% egg yolk powder, 0.2% bile salts, and 78.8% basal feed). Mice in the control group were fed a normal diet. After 10 weeks, mice were randomly assigned to six groups ($n = 10$): control group, model group (HFD), PGZ group (HFD + 10 mg/kg PGZ), low-dose SAL group (SAL-L, HFD + 5 mg/kg), medium-dose SAL group (SAL-M, HFD + 10 mg/kg), and high-dose SAL group (SAL-H, HFD + 20 mg/kg). Mice in the treatment groups were gavaged daily with PGZ or SAL, whereas the control and model groups were administered the same volume of 0.5% CMC-Na for 4 weeks. After treatment, the mice were euthanized under anaesthesia (pentobarbital sodium) after overnight fasting. Serum was obtained by centrifuging blood samples at 6000 rpm for 15 min at 4 °C using a TLD-5013 centrifuge (Anke, Shanghai, China). The liver tissues were collected and divided into two parts. One part of the liver was fixed in 4% paraformaldehyde for histopathological examination, and the other was stored in liquid nitrogen for subsequent experiments.

2.4. AAV8 injection mouse model

After adaptive feeding, 70 mice were randomly divided into seven groups ($n = 10$): control group (normal diet), AAV8-control vectors (AAV8-NC) group (AAV8-ctrl + HFD or AAV8-GFP + HFD), SAL-H group (AAV8-NC + SAL-H + HFD), AAV8-anti-miR-802 group (AAV8-anti-miR-802 + HFD), AAV8-anti-miR-802 + SAL-H group (AAV8-anti-miR-802 + SAL-H + HFD), AAV8-pre-miR-802 group (AAV8-pre-miR-802 + HFD), AAV8-pre-miR-802 + SAL-H group (AAV8-pre-miR-802 + SAL-H + HFD). After 8 weeks of feeding a normal diet or HFD, HFD-fed mice were injected with AAV8-NC or AAV8-miR-802 (1.5×10^{12} v.g.) in 200 μL phosphate-buffered saline (PBS) *via* tail vein. Two weeks later, mice in the SAL-H, AAV8-anti-miR-802 + SAL-H, and AAV8-pre-miR-802 + SAL groups were administered SAL-H (20 mg/kg) by gavage once daily for 4 weeks, whereas the other groups were administered the same volume of 0.5% CMC-Na. Thereafter, the mice were sacrificed, and serum and liver samples were collected. Frozen sections were prepared from each liver tissue sample for fluorescence microscopy to determine the transfection efficiency.

2.5. Serum/hepatic biochemical assays

Serum levels of ALT and AST were determined using an AU480 fully automatic biochemical analyzer (Beckman). TG, TC, LDL-C, and HDL-C levels in the liver were measured using commercially available kits according to the manufacturer's protocols.

2.6. Histopathological examination

A part of the harvested liver tissues was fixed in a 4% paraformaldehyde solution and embedded in paraffin. Paraffin-embedded liver sections were stained with hematoxylin and eosin (H&E) for pathological evaluation. Frozen liver sections were stained with Oil red O and Nile red to evaluate lipid droplet accumulation. The histological features of the liver tissues were observed and captured using the CaseViewer software (3DHISTECH, Hungary).

2.7. Small RNA high-throughput sequencing

Total RNA was extracted from the hepatic tissues of the mice from the control, HFD, and SAL-H groups ($n = 3$ per group) using TRIzol reagent (Invitrogen, #15596018CN). RNA quality was assessed using a NanoPhotometer spectrophotometer (Implen) and an Agilent Bioanalyzer 2100 System (Agilent Technologies). Library for miRNA sequencing was generated using the NEBNext Ultra™ small RNA Sample Library Prep Kit for Illumina (NEB) following the manufacturer's instructions, and library quality was assessed using the Agilent Bioanalyzer 2100 System. Clustering of the index-coded samples was performed using the TruSeq PE Cluster Kit v3-cBot-HS (Illumina). Thereafter, the library preparations were sequenced on the Illumina sequencing platform, and 50-bp single-end reads were generated. Raw data in fastQ were processed using custom Perl and Python scripts and then filtered based on Q20, Q30, and GC content. Next, the obtained clean reads were mapped to the mouse genome and aligned against miRBase to identify the mature miRNAs. The miRNA expression profiles of each sample were analyzed and normalized to transcripts per million using previously described methods[33]. DESeq2 (v1.16.1) was employed to determine differentially expressed miRNAs, with a significance threshold of $P < 0.05$ and absolute foldchange ≥ 2.

2.8. Cell culture and viability

The HepG2, LO2, and Hepa1c1c7 cells were obtained from the American Type Culture Collection. Cells were maintained in

Dulbecco's modified Eagle's medium supplemented with 10% FBS and 1% penicillin/streptomycin, and cultured in an incubator at 37 °C and 5% CO_2. The cells were seeded in 96-well plates and cultured overnight. Then, SAL (5, 10, and 20 μmol/L) was added, and plates were incubated again for 24 h. Three independent replicates were employed for each concentration in each group. Cell viability was determined using a CCK-8 assay.

2.9. Cell treatment and Oil red O staining

HepG2 cells were seeded on glass coverslips in 6-well plates and cultured to 80% confluence. Then, cells were exposed to 1 mmol/L FFA containing sodium oleate and sodium palmitate (2:1) in the presence or absence of SAL (5, 10, and 20 μmol/L). After 24 h, the cells were rinsed twice with PBS and fixed with 4% paraformaldehyde. Next, the cells were soaked in 60% isopropanol and stained with an Oil red O working solution. Stained cells were observed and photographed using an optical microscope. Semi-quantitative analysis was carried out using the ImageJ software. All experiments were repeated thrice.

2.10. Cellular TG and TC activity assays

Following treatment, the primary medium was discarded, and the cells were washed with PBS thrice. Cells were digested with trypsin and centrifuged to obtain the supernatant. The intracellular TG and TC contents in each well were measured using commercial kits following the manufacturer's instructions. The protein levels in each well were quantified using a BCA protein assay kit. All experiments were repeated thrice.

2.11. Cell immunofluorescence assay

For immunofluorescence staining, HepG2 cells were fixed with 4% paraformaldehyde for 15 min and washed thrice with PBS. Subsequently, fixed cells were permeated with 0.3% Triton X-100 for 10 min. After rinsing, 10% goat serum in PBS was added, and the cells were blocked at room temperature for 1 h. Thereafter, the cells were incubated with p-AMPK antibody (1:200, Abcam, #ab32047) at 4 °C overnight. After washing with PBS, the cells were incubated with an Alexa Fluor 488-conjugated anti-rabbit IgG antibody for 1 h at room temperature. Next, the nuclei were stained with 4′,6-diamidino-2-phenylindole for 10 min. After rinsing thrice with PBS, the cells were stained with phalloidin (UElandy, #YP0052S) for 20 min. After washing with PBS, the cells were observed under a fluorescence microscope (Olympus), and the results were analyzed using ImageJ software. All experiments were repeated thrice.

2.12. Dual-luciferase reporter assay

The 3′ untranslated region (UTR) of mouse *Prkab1* from the cDNA of mouse liver was amplified *via* PCR using the primers: forward, 5′-GGACTAGTTGTTGCTTGTTCCAAAAGAAGAGCTC-3′ and reverse, 5′-CCCAAGCTTCAAGTCAGGGTTTTGAAAACAGTAACAAAAG-3′. The *Prkab1* 3′ UTR mRNA was then inserted into the pMIR-Report Luciferase vector to generate the luciferase reporter vector. The *Prkab1* 3′ UTR mut plasmids (forward, 5′-GGACTAGTTGTTGCTTGTTCCAAAAGAAGAGCTC-3′ and mutation reverse, 5′-CCCAAGCTTCAAGTCAGGGTTTTGAAAAGACTTAGAAAAG-3′) were constructed through amplifying and inserting the 3′ UTR mut of the *Prkab1* mRNA into the Luciferase vector. The human *PRKAA1* 3′ UTR and 3′ UTR mut plasmids (forward, 5′-GGACTAGTATAATGTTCCTGATGTTAACAGAAGACTG-3′; reverse, 5′-CCCAAGCTTGCAATATTTAAATATTTTCAAAATAAAACACAGTAACTAAAATG-3′ and mutation reverse, 5′-CCCAAGCTTGCAATATTTAAATATTTTCAAAATAAAACTCTGAATCTAAAATG-3′) were constructed through amplification using the human cDNA and inserting the 3′ UTR and 3′ UTR mut of the *PRKAA1* mRNA into the Luciferase vector, respectively. Reporter assays were performed using mouse Hepa1c1c7 and human HepG2 cells. Cells were seeded in a 24-well plate and cultured for 24 h. Then, cells were transfected with 40 nmol/L miR-802 mimic or mimic control and co-transfected with 0.8 μg of wild-type (WT) 3′ UTR-luc or mutated-type (MUT) 3′ UTR-luc per well using the Lipofectamine 2000 System (Thermo Fisher Scientific). The pGL-4.74 vectors (0.1 μg/well) were co-transfected as the endogenous control for luciferase activity. The luciferase activity was determined after 24 h of transfection using the Dual Luciferase Reporter Gene Assay Kit (Beyotime, #RG029M).

2.13. Small interfering RNA (siRNA) transfection in cells

HepG2 cells (2×10^5 cells/well) were seeded in 6-well plates and classified into seven groups: control, FFA, FFA + SAL, FFA + siPRKAA1, FFA + siPRKAA1 + SAL, FFA + miR-802 inhibitor, and FFA + miR-802 inhibitor + SAL. Non-targeting siRNA and siRNA targeting *PRKAA1* were transiently transfected into HepG2 cells using the EZ Cell Transfection Reagent (Life-iLab, #AC04L092) according to the manufacturer's instructions. Transfecting miR-802 inhibitor or NC inhibitor into HepG2 cell was performed following the manufacturer's protocol. Thereafter, cells were treated with 1 mmol/L FFA and/or SAL (20 μmol/L) for 24 h. Proteins were extracted from the cells for further analysis.

2.14. Quantitative real-time reverse transcription polymerase chain reaction (qRT-PCR)

Total RNA from liver tissues or HepG2 cells was extracted using TRIzol reagent (Sigma, #T9424), and RNA purity was determined using a nanodrop (Allsheng). The RNA was reverse transcribed into cDNA using UEIris II RT-PCR System for First-Strand cDNA Synthesis Kit (US Everbright, #R2028). For miRNA, RNA was reverse transcribed using a miRNA 1st Strand cDNA Synthesis Kit (Vazyme, #MR101-02). qRT-PCR was performed using the Hieff® qPCR SYBR Green Master Mix (YEASEN, #11203ES03) on the QuantStudio™ 5 Real-Time PCR System (Thermo Fisher Scientific). Primer sequences for the mRNAs and miRNAs are listed in Supporting Information Table S1. *Gapdh* and U6 were used as internal reference genes. Relative transcript levels of the test genes were calculated using the $2^{-\Delta\Delta CT}$ method.

2.15. Protein extraction and Western blotting

Proteins were extracted from mouse liver and cells by RIPA lysis buffer (Beyotime Biotechnology) containing protease and phosphatase inhibitors. The BCA protein assay kit was used to measure protein concentration. Protein samples were separated using 10% sodium dodecyl-sulfate polyacrylamide gel electrophoresis and transferred onto a polyvinylidene fluoride membrane. Subsequently, the membrane was blocked with 5% fat-free milk and incubated with primary antibodies against GAPDH (1:40,000),

ACC (1:4000), p-ACC (1:1500), PPARα (1:2000), SREBP-1c (1:2500), PRKAA1 (1:6000), PRKAA2 (1:1200), and PRKAB1 (1:3000) overnight at 4 °C. Membranes were incubated with the corresponding secondary antibodies (1:5000) for 2 h at room temperature. Specific bands were visualized using an enhanced chemiluminescence reagent (Thermo Scientific) and captured using a BioSpectrum Gel Imaging System (UVP). Protein expression was normalized to that of GAPDH.

2.16. *Statistical analysis*

Experimental data are presented as the mean ± standard deviation (SD). Statistical analyses were performed using GraphPad Prism 8.0. Statistical comparisons between different groups were performed using a one-way analysis of variance. $P < 0.05$ was considered statistically significant.

3. Results

3.1. *SAL alleviates lipid accumulation in FFA-treated HepG2 cells*

To evaluate the therapeutic effects of SAL on NAFLD, an FFA-treated HepG2 cell model was established. First, a CCK-8 assay was used to evaluate the cell viability of SAL treatment (5, 10, and 20 μmol/L) in the absence or presence of FFA-treated HepG2 cells and LO2 cells. The results indicated that the concentrations used in this study were safe (Fig. 1A and Supporting Information Fig. S3). Oil red O staining showed that SAL significantly decreased the FFA-treated cellular lipid accumulation in a dose-dependent manner (Fig. 1B). The lipid-lowering effect of SAL was further confirmed by measuring the TG levels in HepG2 cells (Fig. 1C). Notably, SAL dramatically decreased TC content at high doses (Fig. 1D). Therefore, these results suggested that SAL markedly attenuated FFA-treated lipid accumulation in HepG2 cells.

3.2. *SAL regulates lipid metabolism in FFA-treated HepG2 cells*

Owing to the inhibitory effect of SAL on lipid accumulation, we assessed whether SAL affects lipid metabolism-related proteins and gene expression in FFA-treated HepG2 cells. Western blotting analysis showed that SAL treatment significantly decreased SREBP-1c expression and increased PPARα levels compared to those in FFA-treated HepG2 cells (Fig. 2A). Further, qRT-PCR analysis indicated that the upregulation of fat-related synthase genes (*ACC*, *SCD1*, *FAS*, *DGAT1*, and *DGAT2*) and the down-regulation of lipolysis-related gene (*CPT-1*) in FFA-treated HepG2 cells were restored following SAL treatment (Fig. 2B). As AMPK is an important cellular energy sensor that regulates hepatic lipogenesis[10], we further assessed p-AMPK and its downstream protein p-ACC expression to investigate whether SAL exerts its metabolic regulatory activity *via* the AMPK pathway. Immunofluorescence results showed that the fluorescence intensity of p-AMPK in FFA-treated HepG2 cells was significantly decreased, whereas SAL treatment dramatically recovered it (Fig. 2C). Western blotting revealed that FFA exposure reduced p-ACC levels, and this effect was significantly enhanced by SAL (Fig. 2D). Together, these data strongly indicate that SAL inhibits lipid accumulation and promotes β-oxidation *via* activating the AMPK pathway in FFA-treated hepatocytes.

3.3. *SAL alleviates HFD-induced NAFLD in mice*

To examine the effects of SAL on NAFLD, a mouse model was established by feeding mice an HFD for 10 weeks. Subsequently, SAL (5, 10, and 20 mg/kg) was administered orally for another 4 weeks. PGZ was used as a positive control. The histological staining results of H&E, Oil red O, and Nile red showed excessive lipid droplet accumulation, balloon-like changes, hepatocyte swelling and necrosis, and slight inflammatory cell infiltration in the liver of the model group (Fig. 3A). Notably, SAL administration improved these histological changes dose-dependently. In addition, serum ALT and AST and hepatic TG, TC, and LDL-C levels in the model group were remarkably increased, whereas the hepatic HDL-C content was considerably decreased (Fig. 3B). SAL treatment significantly decreased serum ALT and AST and hepatic TG, TC, and LDL-C levels and increased hepatic HDL-C levels compared to those in the model group. In addition, SAL treatment dose-dependently improved the HFD-induced impairment of insulin action and reduced serum IL-6 levels in NAFLD mice (Supporting Information Figs. S4 and S5). Therefore, SAL

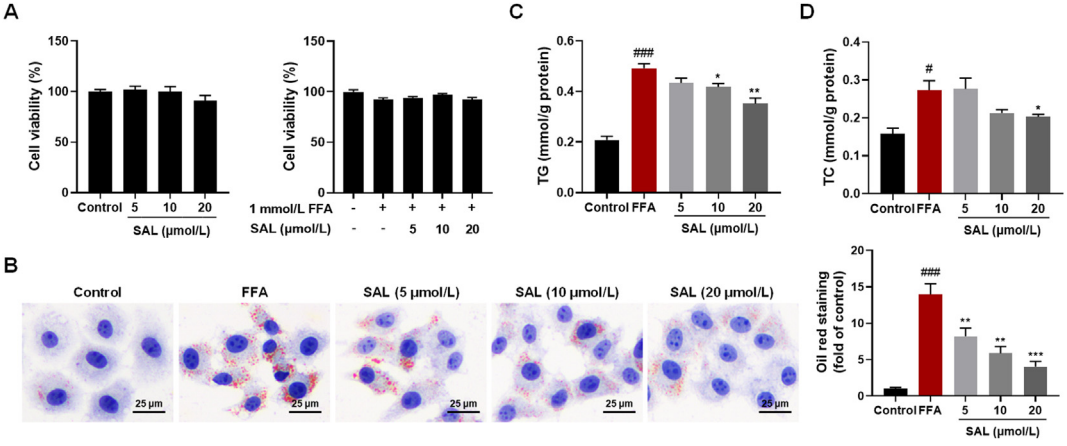

Figure 1 Effect of SAL on lipid accumulation in FFA-treated HepG2 cells. (A) Effects of SAL (5, 10, and 20 μmol/L) on HepG2 cell viability with or without FFA. (B) Lipid droplet deposition in FFA-treated HepG2 cells was assessed using Oil red O staining. Effects of SAL (5, 10, and 20 μmol/L) on TG (C) and TC (D). The data are presented as the mean ± SD ($n = 3$). $^{\#}P < 0.05$, $^{\#\#}P < 0.01$, $^{\#\#\#}P < 0.001$ *vs.* control group; $^{*}P < 0.05$, $^{**}P < 0.01$, $^{***}P < 0.001$ *vs.* model group.

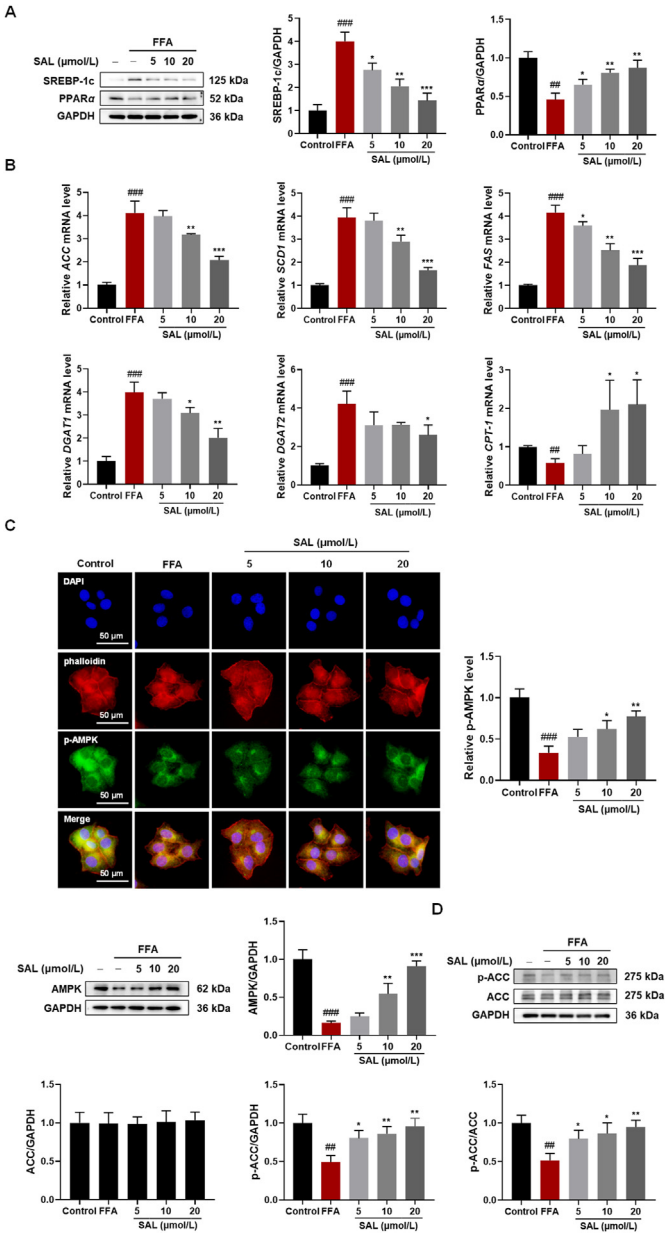

Figure 2 Effect of SAL on lipid accumulation through the AMPK pathway in FFA-treated HepG2 cells. (A) Representative Western blotting results and densitometric analysis of SREBP-1c and PPARα. (B) qRT-PCR analysis of *ACC*, *SCD1*, *FAS*, *DGAT1*, *DGAT2*, and *CPT-1* gene expression. (C) Representative immunofluorescence images of p-AMPK (green) expression and Western blotting analysis of AMPK. Phalloidin (red) and 4',6-diamidino-2-phenylindole (DAPI, blue) were used as cell skeleton and nuclear counterstaining probes, respectively. (D) Representative Western blotting results and densitometric analysis of p-ACC. The results are expressed as the mean ± SD ($n = 3$). $^{\#}P < 0.05$, $^{\#\#}P < 0.01$, $^{\#\#\#}P < 0.001$ *vs.* control group; $^{*}P < 0.05$, $^{**}P < 0.01$, $^{***}P < 0.001$ *vs.* model group.

effectively improved lipid metabolism and liver function in NAFLD mice.

3.4. SAL regulates lipid metabolism via activating the AMPK signaling pathway in NAFLD mice

The cell experiment results indicated AMPK as a key element in SAL, affecting lipid accumulation. Subsequently, *in vivo* experiments were conducted to confirm whether SAL attenuates hepatic steatosis through the AMPK pathway. Western blotting results showed that the protein levels of hepatic p-AMPK were significantly lower in the model group than in the control group (Fig. 4A). In contrast, SAL treatment considerably increased p-AMPK expression dose-dependently. The protein expression of p-ACC, SREBP-1c, and PPARα in the liver was determined to further explore the effect of SAL on the downstream signaling of AMPK. Consistent with the p-AMPK results, a significant reduction in p-ACC and PPARα levels was observed in the model group compared with the control group, whereas their levels were remarkably increased in SAL-treated mice. Conversely, hepatic SREBP-1c expression was significantly increased in the model group, whereas it was notably reduced

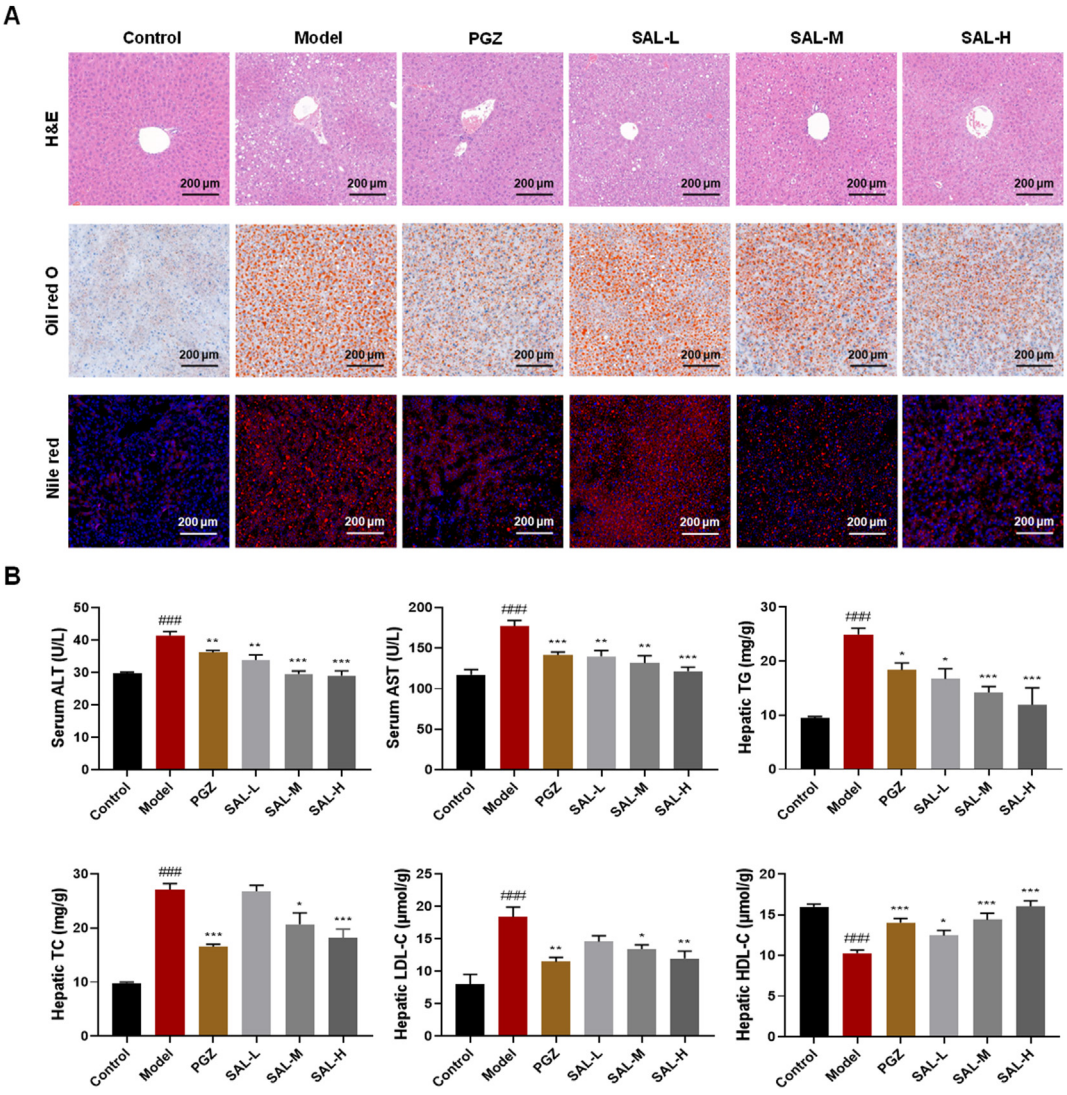

Figure 3 SAL ameliorates hepatic steatosis in HFD-induced NAFLD mice. (A) Representative images of H&E, Oil red O, and Nile red staining of liver sections. (B) Serum ALT and AST and hepatic TG, TC, LDL-C, and HDL-C levels. The results are expressed as the mean ± SD ($n = 6$). $^{\#}P < 0.05$, $^{\#\#}P < 0.01$, $^{\#\#\#}P < 0.001$ *vs.* control group; $^{*}P < 0.05$, $^{**}P < 0.01$, $^{***}P < 0.001$ *vs.* model group.

following SAL treatment. Next, we evaluated the expression of the genes involved in lipogenesis and lipolysis. Notably, the expression of lipogenesis genes (*Acc*, *Scd1*, *Fas*, *Dgat1*, and *Dgat2*) was enhanced, and that of the lipolysis gene (*Cpt-1*) was dramatically decreased in the model group compared with that in the control group (Fig. 4B). SAL treatment inhibited *Acc*, *Scd1*, *Fas*, *Dgat1*, and *Dgat2* and increased *Cpt-1* expression compared with the model group, indicating that it regulates lipid metabolism by activating the AMPK pathway.

3.5. *SAL modulates miR-802 expression to improve lipid metabolism*

To investigate whether miRNAs are involved in the regulatory effects of SAL on lipid accumulation in NAFLD mice, we compared the miRNA profiles of livers from the control, model, and SAL-H groups using miRNA-seq analysis. The replications of the control, model, and SAL-H groups showed satisfactory clustering within their groups, as demonstrated using the principal component analysis (Supporting Information Fig. S6). As shown in Fig. 5A, 51 miRNAs were differentially expressed in the livers of the model and control groups and 55 were differentially expressed between the SAL-H and model groups (Supporting Information Tables S2 and S3). A Venn diagram was used to summarise the differentially expressed miRNAs among groups, and 32 overlapping miRNAs were identified (Fig. 5B). Among them, 20 known mature miRNAs with the opposite expression trends were identified, including seven upregulated and 13 downregulated miRNAs. To determine the potential roles of these 20 miRNAs in ameliorating NAFLD, we predicted the target genes of each miRNA using the TargetScan database and enriched their signaling pathways using the Kyoto Encyclopedia of Genes and Genomes (KEGG) pathway enrichment analysis. As shown in Fig. 5C, the target genes of miR-802 were highly involved in lipid metabolism and the AMPK signaling pathway, indicating the role of miR-802 in alleviating hepatic lipid metabolism disorder in NAFLD mice *via* SAL. Subsequently, qRT-PCR was performed to determine hepatic miR-802 expression in each group. miR-802

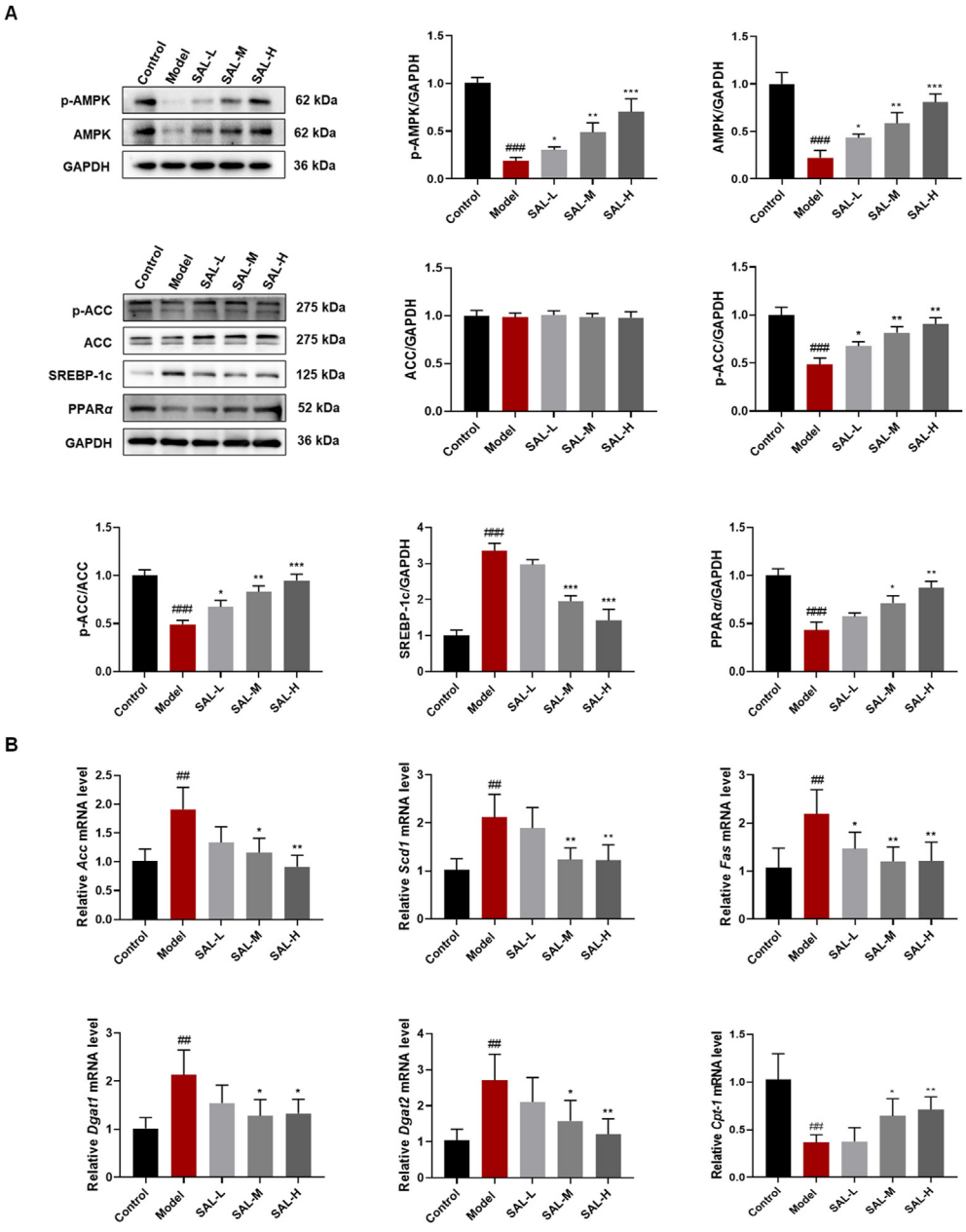

Figure 4 SAL modulates lipid metabolism *via* the AMPK signaling pathway in HFD-induced NAFLD mice. (A) Representative Western blotting results and densitometric analysis of p-AMPK, AMPK, p-ACC, SREBP-1c, and PPARα ($n = 3$). (B) qRT-PCR analysis of *Acc*, *Scd1*, *Fas*, *Dgat1*, *Dgat2*, and *Cpt-1* gene expression ($n = 5$). The results are expressed as the mean ± SD. $^{\#}P < 0.05$, $^{\#\#}P < 0.01$, $^{\#\#\#}P < 0.001$ *vs.* control group; $^{*}P < 0.05$, $^{**}P < 0.01$, $^{***}P < 0.001$ *vs.* model group.

expression was dramatically increased in the model group, and SAL-H treatment significantly reversed this increase (Fig. 5D), which was consistent with the detected and predicted data. Therefore, miR-802 may be an important target of SAL to improve lipid metabolism in NAFLD mice.

3.6. SAL alleviates HFD-induced NAFLD through miR-802 down-regulation

To verify the role of miR-802 in SAL-ameliorated lipid accumulation and hepatic steatosis, NAFLD mice were injected with AAV8 expressing or inhibiting miR-802 *via* the tail vein. Immunohistological analysis showed that more than 80% of hepatocytes of AAV8-anti-miR-802 and AAV8-pre-miR-802 transduced liver tissues display GFP positivity (Supporting Information Fig. S7A), suggesting high efficiency of transduction. Consistently, analysis of miR-802 expression showed that AAV8-anti-miR-802 or AAV8-pre-miR-802 effectively knocked down or overexpressed the miR-802 (Fig. S7B). H&E, Oil red O, and Nile red staining showed that miR-802 suppression in the liver reduced lipid droplet accumulation, balloon-like changes, hepatocyte swelling, and necrosis in NAFLD mice, whereas its overexpression exacerbated these pathological changes (Fig. 6A). Notably, hepatic miR-802 overexpression in NAFLD mice almost

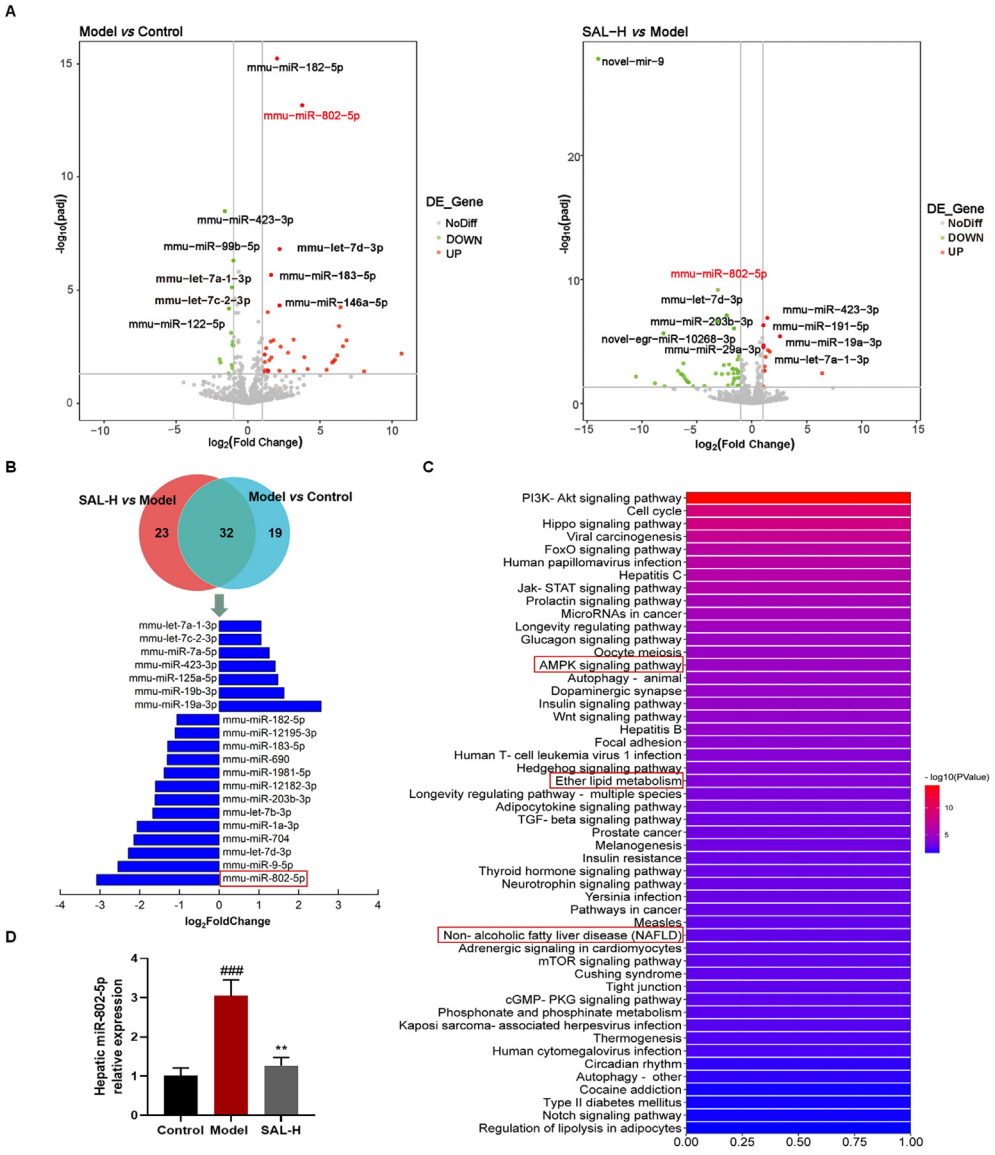

Figure 5 SAL decreases hepatic miR-802 expression in HFD-induced NAFLD mice. (A) Volcanic plots showing the analysis of different genes. (B) Venn diagram verifying different genes among groups, including known mature miRNAs with the opposite expression trend. (C) KEGG signaling pathway analysis of miR-802 target genes. (D) qRT-PCR analysis of miR-802 expression in the livers of mice from the control, HFD, and SAL-H groups ($n = 3$ per group). The results are expressed as the mean ± SD. $^{###}P < 0.001$ *vs.* control group; $^{**}P < 0.01$ *vs.* model group.

abolished the SAL-H-induced improvement in lipid accumulation and hepatic steatosis. Consequently, we examined the effects of miR-802 expression on hepatic TG, TC, LDL-C, and HDL-C levels in NAFLD mice. Consistent with the histological staining results, the abnormal levels of hepatic TG, TC, LDL-C, and HDL-C were effectively reversed by AAV8-anti-miR-802 treatment in NAFLD mice relative to AAV8-NC mice, whereas AAV8-pre-miR-802 treatment dramatically worsened these lipid metabolism-related indicators compared with AAV8-NC mice (Fig. 6B). Compared with the AAV8-NC group, SAL-H treatment resulted in significantly decreased levels of hepatic TG, TC, and LDL-C and increased hepatic HDL-C levels. Expectedly, miR-802 over-expression in the liver almost completely abolished these effects. Therefore, miR-802 downregulation is critical for alleviating HFD-induced NAFLD *via* SAL.

3.7. SAL promotes AMPK pathway activation by inhibiting miR-802 expression

Ppp2ca, *Prkab1*, and *Pafah1b1*, predicted miR-802 target genes, play important roles in lipid metabolism. qRT-PCR results showed that SAL-H treatment significantly decreased hepatic *Prkab1* expression in HFD-induced NAFLD mice but did not affect *Ppp2ca* and *Pafah1b1* expression (Supporting Information Fig. S8), suggesting that SAL activating the AMPK pathway may be achieved by attenuating miR-802-regulated *Prkab1* expression. To further verify whether SAL promotes AMPK pathway activation by inhibiting miR-802 expression, we examined the expression of AMPK signaling pathway-related genes and proteins by transfecting NAFLD mice with AAV8-pre-miR-802 or AAV8-anti-miR-802. PRKAB1, also called AMPKβ1, is a

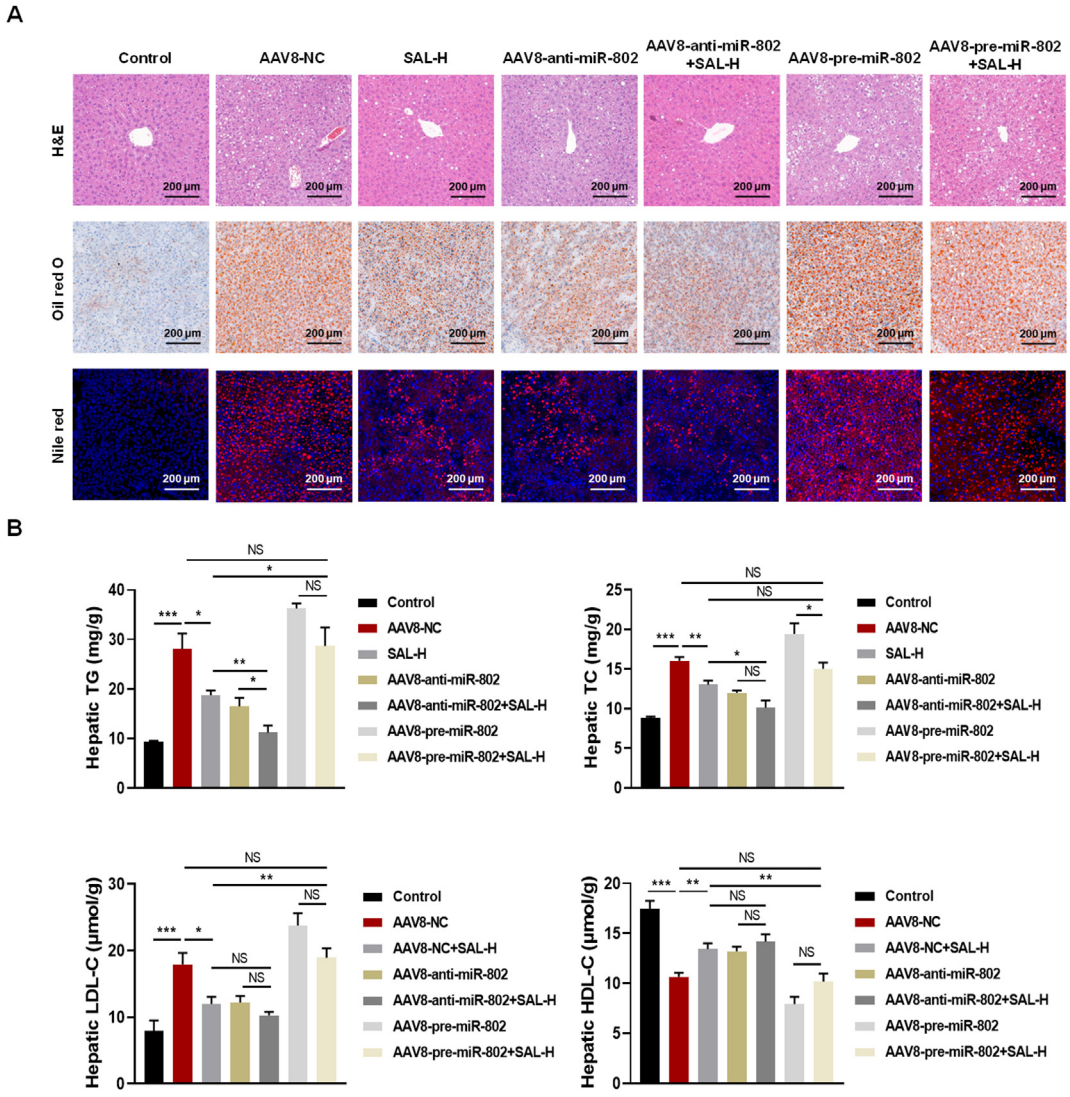

Figure 6 SAL improves hepatic steatosis in HFD-treated mice through downregulating miR-802. (A) Representative images of H&E, Oil red O, and Nile red staining of liver sections. (B) Hepatic TG, TC, LDL-C, and HDL-C levels. The results are expressed as the mean ± SD ($n = 6$). $^{\#}P < 0.05$, $^{\#\#}P < 0.01$, $^{\#\#\#}P < 0.001$ *vs.* control group; $^{*}P < 0.05$, $^{**}P < 0.01$, $^{***}P < 0.001$ *vs.* model group; NS, no significance.

β subunit of AMPK. miR-802 overexpression notably decreased *Prkab1* expression but increased *Acc* and *Fas* expression in the livers of NAFLD mice (Fig. 7A). In contrast, miR-802 suppression significantly increased *Prkab1* expression and decreased *Acc* and *Fas* expression. Similarly, SAL-H treatment significantly increased *Prkab1* expression and decreased *Acc* and *Fas* expression, whereas miR-802 overexpression almost completely abolished these effects. Therefore, SAL potentially functions upstream of miR-802 and regulates *Prkab1* expression. As we all know, *PRKAB1* is a critical bioenergetic sensor that maintains energetic homeostasis *via* activating the α subunits[34]. We speculated that miR-802 regulates *Prkab1* expression and activates PRKAA1 and PRKAA2 in hepatocytes. As expected, hepatic miR-802 knockdown remarkably increased PRKAB1, PRKAA1, and PRKAA2 levels in NAFLD mice, whereas their levels were decreased in the mice in the AAV8-pre-miR-802 group (Fig. 7B). Further, miR-802 overexpression dramatically decreased p-AMPK, p-ACC, and PPARα levels and enhanced SREBP-1c levels in NAFLD mice, whereas miR-802 suppression reversed these changes. Therefore, miR-802 plays a critical role in regulating hepatic lipid metabolism in NAFLD mice through AMPK pathway.

3.8. *miR-802 binds to Prkab1 and regulates its expression*

To determine whether *Prkab1* is a potential target of miR-802, we performed bioinformatics predictions of miRNA targets. Notably, mouse *Prkab1* and human *PRKAA1* exhibit putative miR-802 binding sites in 3' UTR. To confirm miR-802 and *Prkab1*/*PRKAA1* binding, we conducted a luciferase reporter assay using WT or MUT 3' UTR of *Prkab1*/*PRKAA1* (Fig. 8A and B). miR-802 overexpression dramatically decreased luciferase activity in Prkab1-WT, whereas no change was observed in Hepa1c1c7 cells stimulated with mutant 3' UTR. Similarly, in HepG2 cells, miR-802 mimic treatment resulted in the suppression of luciferase intensity in PRKAA1-WT, but this effect was not observed in PRKAA1-MUT, indicating that miR-802

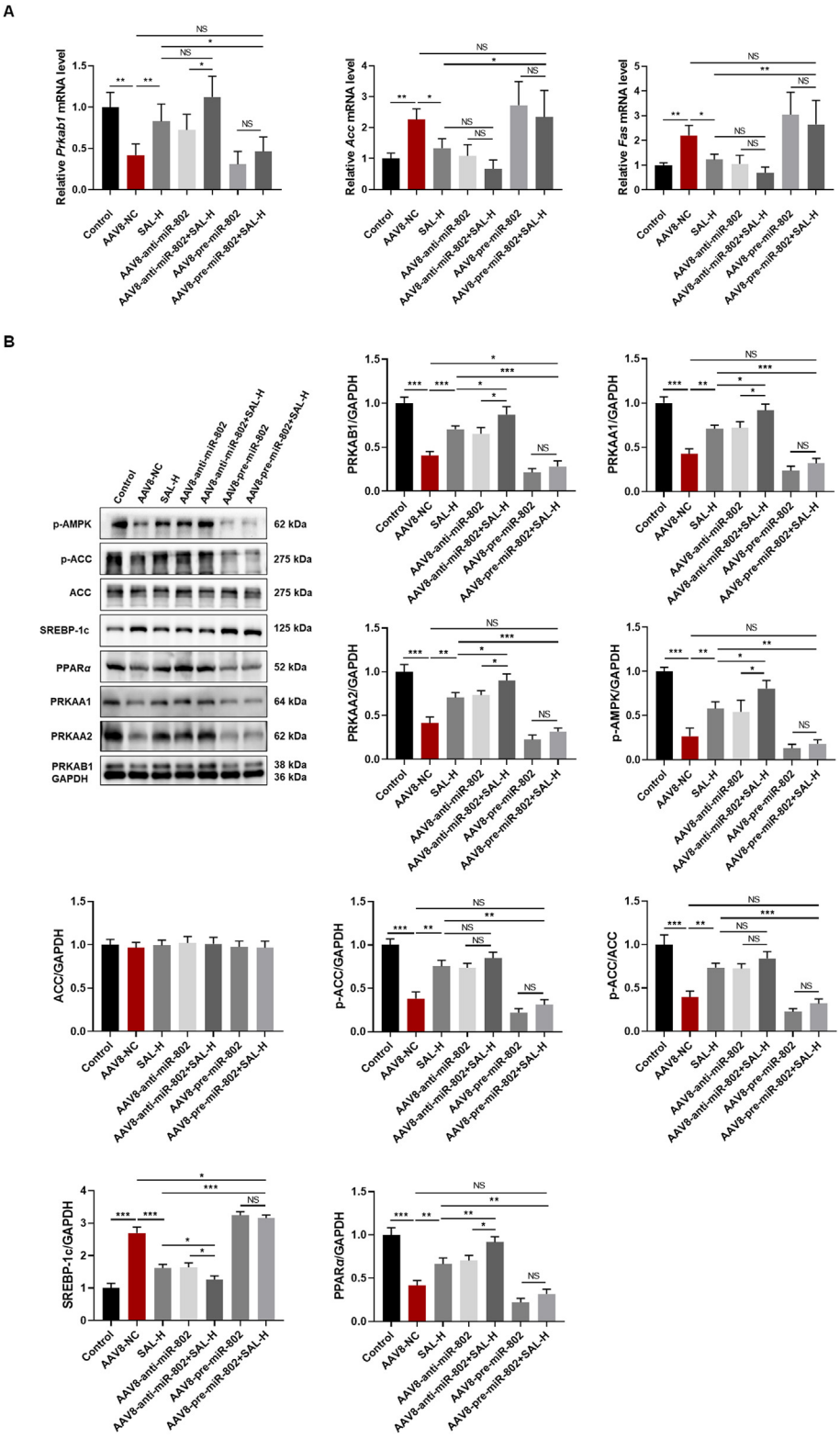

Figure 7 SAL activates the AMPK pathway through miR-802 downregulation. (A) qRT-PCR analysis of *Prkab1*, *Acc*, *and Fas* genes expression ($n = 5$). (B) Representative Western blotting results and densitometric analysis of PRKAB1, PRKAA1, PRKAA2, p-AMPK, p-ACC, SREBP-1c, and PPARα ($n = 3$). The results are expressed as the mean ± SD. $^{\#}P < 0.05$, $^{\#\#}P < 0.01$, $^{\#\#\#}P < 0.001$ *vs.* control group; $^{*}P < 0.05$, $^{**}P < 0.01$, $^{***}P < 0.001$ *vs.* model group; NS, no significance.

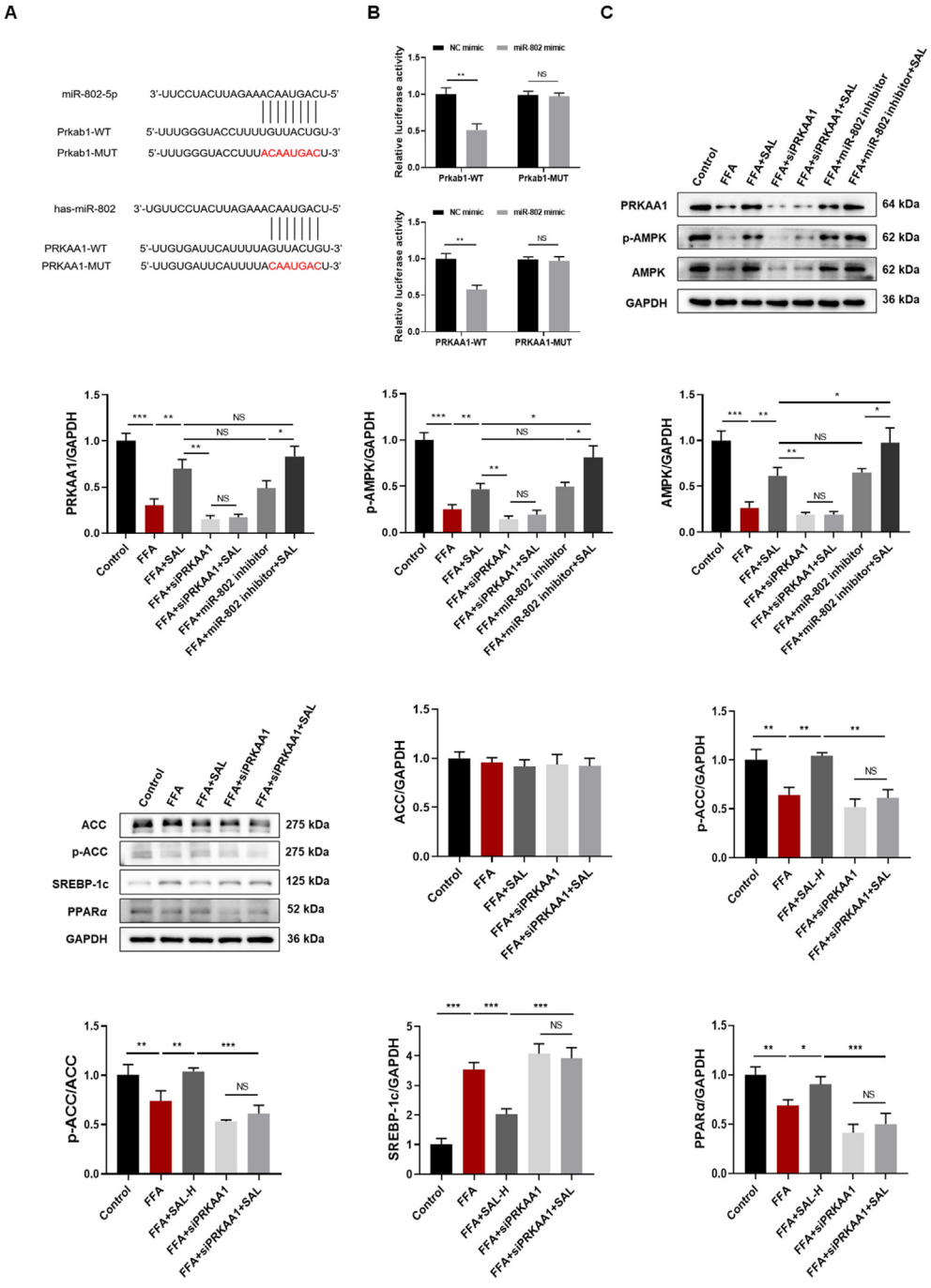

Figure 8 SAL activates AMPK *via* inhibiting miR-802 and its binding to *PRKAA1* or *Prkab1*. (A) Targeted miR-802 and *Prkab1*/*PRKAA1* WT or *Prkab1*/*PRKAA1* Mut sequences. (B) Dual-luciferase reporter assay. (C) Representative Western blotting results and densitometric analysis of PRKAA1, p-AMPK, p-ACC, SREBP-1c, and PPARα. The results are expressed as the mean ± SD (n = 3−5). $^{\#}P < 0.05$, $^{\#\#}P < 0.01$, $^{\#\#\#}P < 0.001$ *vs.* control group; $^{*}P < 0.05$, $^{**}P < 0.01$, $^{***}P < 0.001$ *vs.* model group; NS, no significance.

directly targets mouse *Prkab1* and human *PRKAA1* and suppresses their expression.

3.9. SAL activates the AMPK signaling pathway by inhibiting miR-802 and its binding to PRKAA1

To assess whether SAL activates the AMPK signaling pathway through miR-802 modulation of *PRKAA1*, *PRKAA1* was knocked down in HepG2 cells using siPRKAA1 transfection. Further, *PRKAA1* knockdown was verified using Western blotting (Supporting Information Fig. S9). A significant reduction in PRKAA1 expression was observed in the model group compared with the control group, whereas SAL or/and miR-802 inhibitor treatment remarkably increased PRKAA1 expression (Fig. 8C). In contrast, siPRKAA1 treatment almost completely abolished the enhancement of SAL-induced PRKAA1 expression. Similarly, SAL treatment significantly increased p-AMPK, p-ACC, and PPARα expression and decreased SREBP-1c expression in FFA-

treated HepG2 cells, whereas *PRKAA1* knockdown reversed these changes. Therefore, *PRKAA1* is crucial for AMPK pathway activation by SAL.

4. Discussion

Lipid metabolism dysfunction is the core pathological process involved in NAFLD occurrence and development[8]. Therefore, improving lipid metabolism disorders is an effective strategy for blocking or delaying disease progression[35]. Natural substances exert beneficial effects on hepatic steatosis[36]. In particular, bioactive molecules with low toxicity and lipid-lowering properties have received increasing attention for effectively alleviating NAFLD[37]. In this study, we demonstrated the excellent therapeutic effects of SAL against lipid accumulation and hepatic steatosis in *in vitro* and *in vivo* NAFLD models for the first time. Additionally, we clarified the mechanism underlying the involvement of the miR-802/AMPK axis.

Hepatocyte regulates the primary metabolic and physiological functions of the liver[38]. HepG2 cell line is commonly used to establish the *in vitro* NAFLD model [38]. Although it is a tumor cell type, it possesses the same characteristics as normal human hepatocytes and is easier to culture than primary human hepatocytes[39]. Therefore, the HepG2 cell line was used to study the effects of SAL on lipid metabolism. SAL treatment notably reduced intracellular oil droplets and TG and TC levels in an FFA-treated HepG2 cell model. Further, immunofluorescence and Western blotting showed that SAL significantly up-regulated p-AMPK, p-ACC, and PPARα expression and decreased SREBP-1c expression, suggesting that SAL can improve lipid deposition and activate the AMPK pathway.

The effects of SAL on hepatic steatosis were examined using an HFD-induced NAFLD mouse model. Consistent with previous reports, HFD-fed mice showed notable liver steatosis and damage, accompanied by increased serum AST and ALT and hepatic TG, TC, and LDL-C levels and decreased hepatic HDL-C compared with mice fed a standard chow diet[3,40]. Following SAL intervention, serum AST and ALT and hepatic TG, TC, and LDL-C levels decreased, whereas HDL-C levels increased. In addition, SAL significantly ameliorated HFD-induced hepatic lipid accumulation and steatosis. Therefore, SAL effectively alleviated hepatic steatosis, hepatocyte ballooning, and dyslipidemia and improved liver function in HFD-induced NAFLD mice. Consequently, we explored the underlying therapeutic mechanisms.

A previous study reported that SAL alleviates oxidized LDL-induced endothelial dysfunction *via* an AMPK-dependent mechanism[41]. Notably, AMPK is the master cellular energy sensor that regulates many metabolic processes[42]. Our results revealed that SAL activates the AMPK signaling pathway in an *in vitro* NAFLD model. AMPK is a heterotrimer complex that comprises a catalytic α subunit and two regulatory β and γ subunits[43]. AMPK activation ameliorates NAFLD through multiple mechanisms, including lipid catabolism and lipogenesis inhibition[44]. AMPK phosphorylation inhibits lipid synthesis by inactivating SREBP-1c and ACC[11]. ACC, a crucial lipogenic enzyme, stimulates *de novo* lipogenesis and inhibits fatty acid oxidation[45]. SREBP-1c, a pivotal transcription factor, regulates fatty acid desaturation and lipogenesis-related enzyme expression[46]. In the present study, SAL treatment significantly increased p-AMPK and ACC expression and decreased the expression of SREBP-1c and its target gene, *Fas*, in HFD-induced NAFLD mice. Further, p-AMPK down-regulates SREBP-1c and its target gene, *Fas*, in the NAFLD model[47], which was also observed in the present study. In addition to inhibiting hepatic lipogenesis, p-AMPK also enhances fatty acid β-oxidation by upregulating PPARα-related fatty acid oxidation genes like *Cpt-1*[43]. Fatty acid oxidation is another metabolic pathway that regulates liver lipid homeostasis, and its imbalance results in abnormal TG accumulation and subsequent hepatic steatosis[11]. PPARα is a master factor that controls the β-oxidation of fatty acids, preventing hepatic lipid accumulation by promoting fatty acid catabolism[48]. CPT-1, encoded by *Cpt1*, a target gene of PPARα, is the rate-limiting enzyme in fatty acid oxidation[49]. In this study, SAL treatment significantly increased PPARα and *Cpt-1* levels in mice in the model group. These findings suggested that SAL ameliorates NAFLD by activating the AMPK pathway with subsequent inhibition of SREBP-1c-mediated lipogenesis and the enhancement of PPARα-mediated fatty acid β-oxidation.

Aberrantly expressed miRNAs in the liver are associated with impaired AMPK function in NAFLD[13]. Dysregulated miRNAs in NAFLD inhibit hepatic AMPK expression and activity[50]. As miRNAs are crucial regulators of lipid metabolism, we further explored whether miRNAs are involved in the anti-NAFLD mechanism of SAL using miRNA-seq and bioinformatics analyses. Our study revealed that miR-802 is involved in the AMPK pathway and lipid metabolism, suggesting that miR-802 plays a potential role in the regulation of hepatic lipid metabolism by SAL. Consistent with previous reports, miR-802 expression was dramatically increased in HFD-induced NAFLD mice[34], and SAL treatment significantly decreased its expression. Notably, miR-802 overexpression in NAFLD mice almost completely abolished the SAL-induced improvement in hepatic steatosis. Further, miR-802 knockdown notably improved hepatic steatosis and increased p-AMPK, p-ACC, and PPARα expression, and decreased SREBP-1c expression in NAFLD mice. Collectively, these results revealed that SAL exerted protective effects against NAFLD *via* the miR-802/AMPK axis. miRNAs bind to many mRNAs and modulate their expression[51]. In this study, three target mRNAs (*Ppp2ca*, *Prkab1*, and *Pafah1b1*) of miR-802 were predicted to be involved in lipid metabolism. qRT-PCR results showed that SAL treatment significantly decreased hepatic *Prkab1* expression in HFD-induced NAFLD mice but did not affect *Ppp2ca* and *Pafah1b1* expression. This implies that SAL activates the AMPK pathway by attenuating miR-802-regulated *Prkab1* expression. Further, miR-802 can bind the 3' UTRs of both mouse *Prkab1* and human *PRKAA1*, resulting in decreased AMPK expression and activity[34]. To further examine whether SAL function in lipid accumulation in hepatocytes involves miR-802/PRKAA1, *PRKAA1* was knocked down in HepG2 cells using siPRKAA1. *PRKAA1* knockdown significantly reversed the effects of SAL on p-AMPK, p-ACC, PPARα, and SREBP-1c levels in hepatocytes, suggesting that *PRKAA1* is essential for AMPK pathway activation by SAL. These results suggested that SAL exerts protective effects against NAFLD by modulating miR-802/AMPK-mediated lipid metabolism. In addition, we found that SAL dose-dependently improved the HFD-induced impairment of insulin action in mice. In addition, SAL treatment also reduced serum IL-6 levels in HFD-induced NAFLD mice, suggesting that insulin resistance and pro-inflammatory signaling pathways may also be involved in the anti-NAFLD mechanism of SAL. However, the precise mechanism requires further investigation.

5. Conclusions

This is the first study to demonstrate SAL as an effective therapeutic agent for NAFLD prevention and treatment. The therapeutic effect of SAL was attributed to enhanced lipolysis and fatty acid oxidation, along with its anti-lipogenic activity. Further, SAL exerted protective effects against NAFLD by modulating AMPK-mediated lipid metabolism by inhibiting miR-802. Our findings revealed that, owing to its modulatory effects on the miR-802/AMPK axis, SAL may be a potential leading compound for anti-NAFLD drug development.

Acknowledgments

This work was supported by National Natural Science Foundation of China (Nos. 82304708 and U23A20511); the CAMS Innovation Fund for Medical Sciences (2023-I2M-QJ-013, 2021-I2M-1-031, 2022-I2M-2-002, and 2023-I2M-3-006, China); the Beijing Natural Science Foundation (No. Z220019, China).

Author contributions

Bin Li: Writing − original draft, Methodology, Investigation, Funding acquisition. Qi Xiao: Writing − original draft, Methodology, Investigation. Hongmei Zhao: Methodology, Investigation, Formal analysis. Jianuo Zhang: Investigation. Chunyan Yang: Software, Formal analysis. Yucen Zou: Investigation, Formal analysis. Bengang Zhang: Supervision. Jiushi Liu: Software, Formal analysis. Haitao Sun: Writing − review & editing, Validation, Funding acquisition. Haitao Liu: Writing − review & editing, Supervision, Methodology, Funding acquisition, Formal analysis.

Conflicts of interest

The authors declare no conflicts of interest.

Appendix A. Supporting information

Supporting information to this article can be found online at https://doi.org/10.1016/j.apsb.2024.05.014.

References

1. Scorletti E, Carr RMM. A new perspective on NAFLD: focusing on lipid droplets. *J Hepatol* 2022;**76**:934−45.
2. Song NZ, Xu HJ, Wu SH, Luo SJ, Xu JY, Zhao Q, et al. Synergistic activation of AMPK by AdipoR1/2 agonist and inhibitor of EDPseEBP interaction recover NAFLD through enhancing mitochondrial function in mice. *Acta Pharm Sin B* 2023;**13**:542−58.
3. Inamdar S, Joshi A, Malik S, Boppana R, Ghaskadbi S. Vitexin alleviates non-alcoholic fatty liver disease by activating AMPK in high fat diet fed mice. *Biochem Biophys Res Commun* 2019;**519**:106−12.
4. Huang DQ, El-Serag HB, Loomba R. Global epidemiology of NAFLD-related HCC: trends, predictions, risk factors and prevention. *Nat Rev Gastroenterol Hepatol* 2021;**18**:223−38.
5. Petroni ML, Brodosi L, Bugianesi E, Marchesini G. Management of non-alcoholic fatty liver disease. *BMJ* 2021;**372**:m4747.
6. Li QP, Dou YX, Huang ZW, Chen HB, Li YC, Chen JN, et al. Therapeutic effect of oxyberberine on obese non-alcoholic fatty liver disease rats. *Phytomedicine* 2021;**85**:153550.
7. Katsiki N, Mikhailidis DP, Mantzoros CS. Non-alcoholic fatty liver disease and dyslipidemia: an update. *Metabolism* 2016;**65**:1109−23.
8. Li YP, Liu Y, Chen ZW, Tang KY, Yang LL, Jiang YW, et al. Protopanaxadiol ameliorates NAFLD by regulating hepatocyte lipid metabolism through AMPK/SIRT1 signaling pathway. *Biomed Pharmacother* 2023;**160**:114319.
9. Friedman SL, Neuschwander-Tetri BA, Rinella M, Sanyal AJ. Mechanisms of NAFLD development and therapeutic strategies. *Nat Med* 2018;**24**:908−22.
10. Shen Q, Chen YE, Shi JX, Pei CY, Chen SX, Huang S, et al. Asperuloside alleviates lipid accumulation and inflammation in HFD-induced NAFLD *via* AMPK signaling pathway and NLRP3 inflammasome. *Eur J Pharmacol* 2023;**942**:175504.
11. Askar ME, Ali SI, Younis NN, Shaheen MA, Zaher ME. Raspberry ketone ameliorates nonalcoholic fatty liver disease in rats by activating the AMPK pathway. *Eur J Pharmacol* 2023;**957**:176001.
12. Zhao P, Sun XL, Chaggan C, Liao ZJ, Wong KI, He F, et al. An AMPK−caspase-6 axis controls liver damage in nonalcoholic steatohepatitis. *Science* 2020;**367**:652−60.
13. Sun H, Kemper JK. MicroRNA regulation of AMPK in nonalcoholic fatty liver disease. *Exp Mol Med* 2023;**55**:1974−81.
14. Szabo G. Exosomes and microRNA-223 at the intersection of inflammation and fibrosis in NAFLD. *Hepatology* 2021;**74**:5−8.
15. Gjorgjieva M, Sobolewski C, Dolicka D, Correia de Sousa M, Foti M. MiRNAs and NAFLD: from pathophysiology to therapy. *Gut* 2019;**68**:2065−79.
16. Hochreuter MY, Dall M, Treebak JT, Barrès R. MicroRNAs in non-alcoholic fatty liver disease: progress and perspectives. *Mol Metab* 2022;**65**:101581.
17. Sun Y, Shen YM, Liang XR, Zheng HL, Zhang YT. MicroRNAs as biomarkers and therapeutic targets for nonalcoholic fatty liver disease: a narrative review. *Clin Ther* 2023;**45**:234−47.
18. Di Mauro S, Scamporrino A, Filippello A, Di Pino A, Scicali R, Malaguarnera R, et al. Clinical and molecular biomarkers for diagnosis and staging of NAFLD. *Int J Mol Sci* 2021;**22**:11905.
19. Dávalos A, Goedeke L, Smibert P, Ramírez CM, Warrier NP, Andreo U, et al. miR-33a/b contribute to the regulation of fatty acid metabolism and insulin signaling. *Proc Natl Acad Sci U S A* 2011;**108**:9232−7.
20. Meng XY, Guo J, Fang WW, Dou L, Li M, Huang XQ, et al. Liver microRNA-291b-3p promotes hepatic lipogenesis through negative regulation of adenosine 5′-monophosphate (AMP)-activated protein kinase α1. *J Biol Chem* 2016;**291**:10625−34.
21. Xu YY, Zhu YD, Hu SW, Pan XL, Bawa FC, Wang HH, et al. Hepatocyte miR-34a is a key regulator in the development and progression of non-alcoholic fatty liver disease. *Mol Metab* 2021;**51**:101244.
22. Li B, Xiao Q, Liu JS, Mu XL, Zhang JN, Qi YD, et al. Chemical characterization and potential mechanism of the anti-asthmatic activity of a subfraction from *Schisandra chinensis* fruit extract. *J Agric Food Chem* 2022;**70**:5015−25.
23. Deng L, Cheng S, Li J, Xu X, Hao X, Fan Y, et al. Synthesis and biological evaluation of novel schisanhenol derivatives as potential hepatoprotective agents. *Eur J Med Chem* 2022;**227**:113919.
24. Yu WJ, Chen CZ, Peng YX, Li Z, Gao Y, Liang S, et al. Schisanhenol improves early porcine embryo development by regulating the phosphorylation level of MAPK. *Theriogenology* 2021;**175**:34−43.
25. Yang H, Li L, Jiao Y, Zhang Y, Wang Y, Zhu K, et al. Thioredoxin-1 mediates neuroprotection of schisanhenol against MPP^+-induced apoptosis *via* suppression of ASK1−P38−NF-κB pathway in SH-SY5Y cells. *Sci Rep* 2021;**11**:21604.
26. He T, Wang QY, Shi JZ, Fan TY, Yan C, Huang LJ, et al. Synthesis and the hepatoprotective activity of dibenzocyclooctadiene lignan derivatives. *Bioorg Med Chem Lett* 2014;**24**:1808−11.
27. He XL, Chen JM, Mu YP, Zhang H, Chen GF, Liu P, et al. The effects of inhibiting the activation of hepatic stellate cells by lignan components from the fruits of *Schisandra chinensis* and the mechanism of schisanhenol. *J Nat Med* 2020;**74**:513−24.
28. Gu M, Feng Y, Chen Y, Fan S, Huang C. Deoxyschizandrin ameliorates obesity and non-alcoholic fatty liver disease: involvement of dual

farnesyl X receptor/G protein-coupled bile acid receptor 1 activation and leptin sensitization. *Phytother Res* 2023;**37**:2771−86.
29. Yan LS, Zhang SF, Luo G, Cheng BC, Zhang C, Wang YW, et al. Schisandrin B mitigates hepatic steatosis and promotes fatty acid oxidation by inducing autophagy through AMPK/mTOR signaling pathway. *Metabolism* 2022;**131**:155200.
30. Li B, Xiao Q, Zhang JN, Wang YM, Liu JS, Zhang BG, et al. Exploring the active compounds and potential mechanism of the anti-nonalcoholic fatty liver disease activity of the fraction from *Schisandra chinensis* fruit extract based on multi-technology integrated network pharmacology. *J Ethnopharmacol* 2023;**301**:115769.
31. Zhou ZY, Li YM, Ma XF, Cao BY, Peng T, Sheng YW, et al. Identification of a novel TAR RNA-binding protein 2 modulator with potential therapeutic activity against hepatocellular carcinoma. *J Med Chem* 2021;**64**:7404−21.
32. Xue LJ, Liu KQ, Yan CX, Dun J, Xu YX, Wu LL, et al. *Schisandra* lignans ameliorate nonalcoholic steatohepatitis by regulating aberrant metabolism of phosphatidylethanolamines. *Acta Pharm Sin B* 2023;**13**:3545−60.
33. Zhou L, Chen JH, Li ZZ, Li XX, Hu XD, Huang Y, et al. Integrated profiling of microRNAs and mRNAs: microRNAs located on Xq27.3 associate with clear cell renal cell carcinoma. *PLoS One* 2010;**5**:e15224.
34. Ni YY, Xu ZP, Li C, Zhu YX, Liu R, Zhang F, et al. Therapeutic inhibition of miR-802 protects against obesity through AMPK-mediated regulation of hepatic lipid metabolism. *Theranostics* 2021;**11**:1079−99.
35. Vitulo M, Gnodi E, Rosini G, Meneveri R, Giovannoni R, Barisani D. Current therapeutical approaches targeting lipid metabolism in NAFLD. *Int J Mol Sci* 2023;**24**:12748.
36. Cheng C, Li ZZ, Zhao X, Liao CL, Quan J, Bode AM, et al. Natural alkaloid and polyphenol compounds targeting lipid metabolism: treatment implications in metabolic diseases. *Eur J Pharmacol* 2020;**870**:172922.
37. Yan TT, Yan NN, Wang P, Xia YL, Hao HP, Li GJ, et al. Herbal drug discovery for the treatment of nonalcoholic fatty liver disease. *Acta Pharm Sin B* 2020;**10**:3−18.
38. Wang MY, Zhang SS, An MF, Xia YF, Fan MS, Sun ZR, et al. Neferine ameliorates nonalcoholic steatohepatitis through regulating AMPK pathway. *Phytomedicine* 2023;**114**:154798.
39. Ni HY, Yu L, Zhao XL, Wang LT, Zhao CJ, Huang H, et al. Seed oil of *Rosa roxburghii* Tratt against non-alcoholic fatty liver disease *in vivo* and *in vitro* through PPARα/PGC-1α-mediated mitochondrial oxidative metabolism. *Phytomedicine* 2022;**98**:153919.
40. Li FF, Jiang M, Ma MH, Chen XY, Zhang YD, Zhang YX, et al. Anthelmintics nitazoxanide protects against experimental hyperlipidemia and hepatic steatosis in hamsters and mice. *Acta Pharm Sin B* 2022;**12**:1322−38.
41. Chiu TH, Ku CW, Ho TJ, Tsai KL, Hsu WC, Chen YA, et al. Schisanhenol attenuates oxLDL-induced endothelial dysfunction *via* an AMPK-dependent mechanism. *Am J Chin Med* 2023;**51**:1459−75.
42. Steinberg GR, Hardie DG. New insights into activation and function of the AMPK. *Nat Rev Mol Cell Biol* 2023;**24**:255−72.
43. Day EA, Ford RJ, Steinberg GR. AMPK as a therapeutic target for treating metabolic diseases. *Trends Endocrinol Metab* 2017;**28**:545−60.
44. Hardie DG, Ross FA, Hawley SA. AMPK: a nutrient and energy sensor that maintains energy homeostasis. *Nat Rev Mol Cell Biol* 2012;**13**:251−62.
45. Mao J, DeMayo FJ, Li H, Abu-Elheiga L, Gu Z, Shaikenov TE, et al. Liver-specific deletion of acetyl-CoA carboxylase 1 reduces hepatic triglyceride accumulation without affecting glucose homeostasis. *Proc Natl Acad Sci U S A* 2006;**103**:8552−7.
46. Horton JD, Goldstein JL, Brown MS. SREBPs: activators of the complete program of cholesterol and fatty acid synthesis in the liver. *J Clin Invest* 2002;**109**:1125−31.
47. Liao CC, Ou TT, Huang HP, Wang CJ. The inhibition of oleic acid induced hepatic lipogenesis and the promotion of lipolysis by caffeic acid *via* up-regulation of AMP-activated kinase. *J Sci Food Agric* 2014;**94**:1154−62.
48. Tian X, Ru Q, Xiong Q, Wen RJ, Chen Y. Catalpol attenuates hepatic steatosis by regulating lipid metabolism *via* AMP-activated protein kinase activation. *Biomed Res Int* 2020;**2020**:6708061.
49. Mascaro C, Acosta E, Ortiz JA, Marrero PF, Hegardt FG, Haro D. Control of human muscle-type carnitine palmitoyltransferase I gene transcription by peroxisome proliferator-activated receptor. *J Biol Chem* 1998;**273**:8560−3.
50. Long JK, Dai W, Zheng YW, Zhao SP. miR-122 promotes hepatic lipogenesis *via* inhibiting the LKB1/AMPK pathway by targeting Sirt1 in nonalcoholic fatty liver disease. *Mol Med* 2019;**25**:26.
51. Lewis BP, Burge CB, Bartel DP. Conserved seed pairing, often flanked by adenosines, indicates that thousands of human genes are microRNA targets. *Cell* 2005;**120**:15−20.